Particle-in-cell simulations of multiple ionization of small molecules in a strong laser field

Kenichi Ishikawa* and Thomas Blenski
Service des Photons, Atomes et Molécules, Centre d'Etudes Nucléaires de Saclay, Commissariat à l'Energie Atomique, 91191 Gif-sur-Yvette Cedex, France
(Received 30 June 1999; published 10 May 2000)

We present one-dimensional particle-in-cell simulations of multielectron dissociative ionization (MEDI) of diatomic and linear triatomic molecules exposed to an intense subpicosecond laser pulse. Our method allows us to deal with all the electrons and nuclei explicitly, and to follow the temporal evolution of MEDI. The simulation results confirm that ionization probability is strongly enhanced at a certain critical internuclear distance. This occurs when the internal potential barriers surpass the external one and electrons are localized in higher potential wells. The mechanism of enhanced ionization in a diatomic and a triatomic molecule can be understood in a similar way, though all three potential wells participate in it for the triatomic case. Nevertheless, the occurrence of ionization is not necessarily localized at the critical distance. In addition, our simulations show that there is no significant difference in the final charge state of ion fragments between diatomic and linear triatomic molecules. The relative smallness of the critical distance in our results may suggest that not only the ionization taking place preferably near the critical distance, but also the non-Coulombic nature of the molecular potential curves, cause the experimentally observed kinetic-energy defects.

PACS number(s): 33.80.Rv, 31.15.Lc, 33.80.Eh, 82.50.Fv

I. INTRODUCTION

Since the advent of high-intensity ($>10^{14}$ W/cm^2), short-pulse (<1 ps) lasers, there has been growing interest in the study of intense laser interaction with molecules. Molecules exposed to a strong laser field undergoes a process called multielectron dissociative ionization (MEDI) [1–5], in which multiple ionization is accompanied by dissociation. Since the ionization process is generally faster than the dissociation process at such high intensities, the simplest model of MEDI may be the Coulomb explosion: (in the case of a diatomic molecule) the total kinetic energy of resulting ion fragments of charges q_1 and q_2 is given by $E_{\mathrm{coul}} = q_1 q_2 / R_e$, where R_e is the equilibrium internuclear distance of the molecule. Experiments have revealed, however, that the measured kinetic energy E_{expt} is lower than this for all fragmentation channels (the difference $E_{\mathrm{coul}} - E_{\mathrm{expt}}$ is called the kinetic-energy defect), and that the ratio $E_{\mathrm{expt}}/E_{\mathrm{coul}}$ does not depend much on laser wavelength or pulse duration in spite of the potential complexity of the phenomena. These results have led experimentalists to speculate that ionization to higher charge states takes place preferably at a certain effective distance given by $(E_{\mathrm{coul}}/E_{\mathrm{expt}})R_e$ [4].

Theoretical modeling of the ionization of molecules in intense laser fields is a challenging subject involving the nonlinear, nonperturbative response. Several authors [6–11] found a possible explanation for the above experimental findings: the ionization probability of molecular ions depends on internuclear distance, and strongly peaks at a certain critical distance R_c larger than R_e, and the value of R_c does not vary significantly between subsequent ionization stages. Most of this work, however, used a single active electron approximation and was, therefore, strictly applicable only for one-electron molecular ion such as H_2^+, while the production of multiply charged ions has by its nature a many-electron character. The first theoretical work to treat all the electrons was probably that of Brewczyk and coworkers [12–14]. They solved hydrodynamic equations for electron cloud based on one- and two-dimensional time-dependent Thomas-Fermi models. Their results raised a question as to the genuineness of enhanced ionization, and they instead suggested that the screening of the escaping ion fragments by ejected electrons may be responsible for the kinetic-energy defect. This qualitative discrepancy between the outcomes of the two groups of models has motivated us to develop an alternative dynamical model of MEDI.

In this paper we present one-dimensional particle-in-cell (PIC) simulations of MEDI of a Cl_2 molecule in an intense laser field, based on the Vlasov equation. The electron cloud is represented as an assembly of classical test particles, each of which moves according to Newton's equations of motion. The motion of the test particles models the evolution of the electron distribution function in phase space. The effect of quantum mechanics is taken into account only in the initial electron-density distribution calculated with one-dimensional Thomas-Fermi theory. Although the interaction of electromagnetic fields with atoms and molecules requires, in principle, quantum-mechanical treatments, classical treatments have been successfully applied in case of intense laser fields [15–19]. In our model we need not fix the nuclei. Thus our method allows us to follow the temporal evolution of MEDI. Our simulations reconfirm the enhancement of ionization probability in a certain range of internuclear distance. This can be connected to the rise of the internal potential barrier and the resulting nonadiabatic electron localization in one potential well. On the other hand, the results of the present study do not support the idea of the ejected-electron screening of ion fragments proposed in Refs. [12–14].

Furthermore, we apply our PIC method to a linear tri-

*Author to whom correspondence should be addressed. Electronic address: ishikawa@cea.fr

atomic molecule. Hering and Cornaggia [20] in their experiments compared ion yields in the laser-induced multiple ionization of CO, O_2, and N_2 with those of CO_2, CO_2, and N_2O, respectively, and found that the multicharged-ion production is similar for the diatomic and linear triatomic molecules. On the theoretical side, Seideman *et al.* [21] studied the multiple ionization of a triatomic molecule using one-dimensional quantum-mechanical calculations with a single active electron approximation, and showed that the ionization rate of a triatomic molecule increases dramatically as either bond or both bonds are stretched to the same critical distance observed in the diatomic case. Their results indicate that the lowest two potential wells are involved in the enhanced ionization. In Ref. [21], however, the ionization efficiency of a triatomic molecule is not compared explicitly with that of a diatomic molecule. In order to compare the ionization behavior of diatomic and triatomic molecules directly, we simulate the MEDI of a fictitious Cl_3 molecule. We again find enhanced ionization at a certain internuclear distance again. Its mechanism is similar to that in a diatomic molecule but is slightly different from that in Ref. [21], as we will discuss below. Moreover, our results show that the enhanced ionization is triggered at a smaller internuclear distance than in the diatomic case.

The present paper is organized as follows. Section II describes our simulation method. After the brief summary of the PIC method, we discuss the initial test particle distribution in phase space. In Sec. III we apply the method to the MEDI of a Cl_2 molecule in an intense laser field. In particular, we discuss the ionization probability enhancement in detail. In this section the comparison of our results with those of the hydrodynamic model is also included. In Sec. IV we apply our simulation method to the MEDI of a fictitious Cl_3 molecule, and discuss the mechanism of ionization enhancement in a linear triatomic molecule. The conclusions are given in Sec. V. We briefly mention the scaling property of our model in the Appendix.

II. SIMULATION METHOD

In this section we describe our simulation method of multiple ionization of a diatomic molecule. Its extension to a linear triatomic molecule is straightforward.

A. Dynamical model

We consider a diatomic molecule aligned along with the electric-field vector of linearly polarized laser light. The alignment is believed to occur in strong-field laser irradiation of diatomic molecules [6,7,22–24]. In order to simplify the calculations, we confine the motion of electrons and nuclei in one dimension. One-dimensional theoretical models have been used in the study of intense-field interaction with atoms [25–27] and H_2^+ molecules [28], and have turned out to be able to account for the essential relevant physics. We expect that one-dimensional approximations are more reliable in the case of aligned diatomic molecules.

In our model, the electron cloud is represented by an assembly of N_p identical test particles. Each test particle has a mass $m_p=2Z/N_p$ and a charge $q_p=-2Z/N_p$, where Z is the charge number of the nuclei. We use atomic units throughout this paper unless otherwise stated. The position and velocity of test particle i are denoted by x_i and v_i, respectively. Test particles have the same charge-to-mass ratio as electrons. In order to generate the electron density $\rho(x)$ from particle positions, we introduce N_g space-fixed grids of step Δx. The density ρ_j on grid $j(j=1,\ldots,N_g)$, whose position is X_j, is calculated as

$$\rho_j=\frac{2Z}{N_p}\sum_{i=1}^{N_p} S(x_i-X_j), \tag{1}$$

where $S(x)$ is a weighting function which satisfies $\Delta x\Sigma_{j=1}^{N_g}S(x-X_j)=1$ for any x. In the present study, we use the third-order Spline function [29]. The motion of test particles is governed by Newton's equations

$$\frac{dx_i}{dt}=v_i, \quad \frac{dv_i}{dt}=f_i=-\frac{\partial}{\partial x}\Phi_{\rm eff}(x_i,t). \tag{2}$$

Here the effective potential $\Phi_{\rm eff}(x_i,t)$ is given by

$$\Phi_{\rm eff}(x,t)=-\frac{Z}{\sqrt{b^2+(x-x_L)^2}}-\frac{Z}{\sqrt{b^2+(x-x_R)^2}} + \int_{-\infty}^{\infty}\frac{\rho(x')}{\sqrt{c^2+(x-x')^2}}dx'+xE(t), \tag{3}$$

where b and c are smoothing parameters which are commonly used in one-dimensional models to remove the Coulomb singularity [27], x_L and x_R are the positions of the first (left) and second (right) nuclei, respectively, and $E(t)$ is the laser electric field. In practice, the effective potential is evaluated only on grids from ρ_j and $E(t)$ by use of fast Fourier transform. Let us denote its value on grid j by $\Phi_{{\rm eff},j}$. The force f_i acting on an ith test particle can be evaluated either with the momentum-conserving expression [29]

$$f_i=\sum_{j=1}^{N_g} S(x_i-X_j)F_j, \tag{4}$$

where

$$F_j=-\frac{\Phi_{{\rm eff},j+1}-\Phi_{{\rm eff},j-1}}{2\Delta x}, \tag{5}$$

or with the energy-conserving expression [29]

$$f_i=-\Delta x\sum_{j=1}^{N_g}\Phi_{{\rm eff},j}\frac{\partial}{\partial x_i}S(x_i-X_j). \tag{6}$$

The results presented in the present paper are obtained with the energy-conserving algorithm. We have found that the use of the momentum-conserving algorithm yields virtually the same results. The motion of the nuclei is calculated also from Newton's equations.

$$\frac{dx_{L,R}}{dt}=v_{L,R}, \quad \frac{dv_{L,R}}{dt}=\frac{f_{L,R}}{M}, \tag{7}$$

where M is the nuclear mass. The force f_L acting on the left nucleus, for example, is calculated from

$$f_L=\frac{Z^2(x_L-x_R)}{|x_L-x_R|^3}-\int_{-\infty}^{\infty}\frac{Z\rho(x')(x_L-x')}{[b^2+(x_L-x)^2]^{3/2}}dx'+ZE(x_L). \tag{8}$$

Using thus evaluated forces f_L, f_R, and f_i $(i=1,\ldots,N_p)$, we calculate the new values of x_L, x_R, and x_i by integrating the equations of motion in a time step Δt. In the present study the Verlet method [30] is employed for the time integration, though the use of the leap-frog method [29] does not affect results much. We proceed to the next time step by beginning again with density weighting Eq. (1).

Let us briefly remark on the connection between the present method and time-dependent density-functional theory. The simulation method described above belongs to the category of the PIC method, which is widely used in plasma physics [29] and intense-laser interaction with solids [31]. The test particles can be regarded as Lagrangian markers embedded randomly in the electron gas whose evolution is described by the kinetic Vlasov equation, and moving with it through phase space [32]. Although the Vlasov equation is of relevance to classical particles, it can be also derived as the leading order of a semiclassical $\hbar$ expansion of the time-dependent Kohn-Sham equations [33–35].

B. Initial particle distribution

While test particles and nuclei move according to the classical equations of motion, the effects of quantum mechanics are partially taken into account in the initial distribution of test particles.

The positions x_i of test particles are initially distributed according to the ground-state density of the molecule, calculated using the one-dimensional Thomas-Fermi model [12,13]. In this model, the total energy of the molecule is expressed as

$$\mathcal{E}[\rho,R]=\mathcal{E}_{\rm kin}+\mathcal{E}_{\rm en}+\mathcal{E}_{\rm ee}, \tag{9}$$

where

$$\mathcal{E}_{\rm kin}=A\int\rho^2(x)dx, \tag{10}$$

$$\mathcal{E}_{\rm en}=-\int\frac{Z}{\sqrt{(x-R/2)^2+b^2}}dx-\int\frac{Z}{\sqrt{(x+R/2)^2+b^2}}dx, \tag{11}$$

$$\mathcal{E}_{\rm ee}=\frac{1}{2}\int\int\frac{\rho(x)\rho(x')}{\sqrt{(x-x')^2+c^2}}dxdx'. \tag{12}$$

Here R is the internuclear distance, b and c are the smoothing parameters that already appeared in Eq. (3), and A is a universal constant. The minimization of the energy functional [Eq. (9)] with respect to $\rho(x)$ with the constraint that the system contains a fixed number of electrons, leads to the following coupled equations:

$$\Phi(x)+2A\rho(x)=\Phi_0, \tag{13}$$

$$\Phi(x)=-\frac{Z}{\sqrt{b^2+(x-R/2)^2}}-\frac{Z}{\sqrt{b^2+(x+R/2)^2}}+\int_{-\infty}^{\infty}\frac{\rho(x')}{\sqrt{c^2+(x-x')^2}}dx'. \tag{14}$$

A constant Φ_0 vanishes in the case of neutral molecules. Since Eqs. (13) and (14) are linear, they can be solved using the Fourier transform technique. By minimizing $\mathcal{E}$ further with respect to R, one obtains the equilibrium internuclear distance R_e.

We apply this model to a Cl_2 $(Z=17, M=6.24\times10^4)$ molecule. The values of A, b, and c are determined in such a way that they give reasonable physical properties of the diatomic molecules, such as binding energies and equilibrium internuclear separations. Brewczyk and co-workers [12,13] found that the parameter set $A=0.3$, $b=1.22$, and $c=1.65$ yields the equilibrium internuclear separation $R_e=3.8$ a.u. and the binding energy $D=0.11$ a.u., in agreement with the experimental values [36] $R_e=3.76$ a.u. and $D=0.091$ a.u. We use this parameter set.

As an initial electron distribution $f(\mathbf{r},\mathbf{v})$ in phase space, we choose the following stationary solution of the Vlasov equation [33]:

$$f(\mathbf{r},\mathbf{v})=C\,\theta(E_F-[v^2/2+\Phi(\mathbf{r})]), \tag{15}$$

where E_F is the Fermi energy, and C is a constant. This distribution does not yield the kinetic-energy density of the form $A\rho^2$ as in Eq. (10) in one dimension. In fact, the one-dimensional version of Eq. (15) leads to a kinetic-energy density proportional to ρ^3. Brewczyk and co-workers [12,13] chose the form $A\rho^2$ by experimentation with possible forms of the kinetic-energy functional. This choice can be reconciled with Eq. (15) through the following considerations. We assume that the velocity of electrons is distributed virtually in two dimensions, i.e.,

$$f(x,v_x,v_y)=\frac{1}{4\pi A}\,\theta(-\Phi(x)-(v_x^2+v_y^2)/2). \tag{16}$$

For neutral molecules E_F vanishes, and the coefficient $1/(4\pi A)$ has been determined so that Eq. (10) is satisfied. It should be emphasized that the introduction of v_y, the y component of the velocity, is nothing more than a mathematical trick to construct a stable initial state of a model molecule. Time evolution is considered exclusively in one dimension (the x direction), and the y component of the velocity of test particles is assumed not to change in time.

In the present dynamical model, the distribution given by Eq. (16) will decay into a Maxwell-Boltzmann distribution in practice through collisions between test particles, and it is a stationary state only in the limit of a large number of test

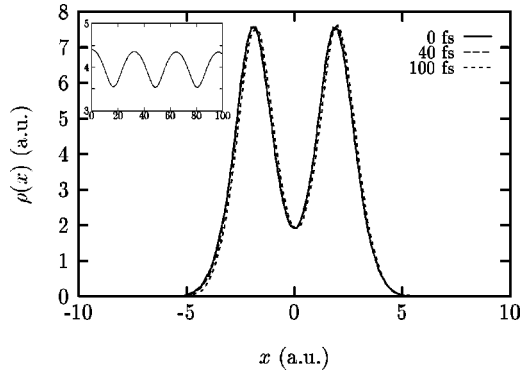

FIG. 1. Calculated electron density distribution $\rho(x)$ in the absence of laser field at $t=0$ fs (solid line), 40 fs (dashed line), and 100 fs (dotted line). Inset: Internuclear distance (a.u.) as a function of time (fs) for free oscillations of Cl_2 for small internuclear excursions away from R_e.

particles. In Fig. 1 we plot the electron density $\rho(x)$ in the model Cl_2 molecule for three different times. The electron cloud consists of 500 000 test particles which are randomly distributed in phase space according to Eq. (16) at $t=0$. $\rho(x)$ remains virtually unchanged for 100 fs, except for small fluctuations and a slight drift of the whole molecule. The results shown in what follows have been obtained with the test particle number $N_p=500\,000$ unless otherwise stated. As a simple check of the dynamical model, we have verified that it reproduces molecular vibrations in the absence of laser fields as is shown in the inset of Fig. 1, which displays the free oscillation of the internuclear distance $R(t)$. The period of oscillation (34 fs) is shorter than the experimental value (59 fs) [36]. The present model overestimates the stiffness of the molecular potential. These results are similar to those obtained from the time-dependent Thomas-Fermi model (see Fig. 1 of Ref. [12]).

III. COULOMB EXPLOSION OF DIATOMIC MOLECULES IN AN INTENSE LASER FIELD

We have performed the PIC simulations for a model Cl_2 molecule in an intense subpicosecond laser pulse. The shape of the laser-field envelope is chosen to be proportional to sine squared.

Figure 2 shows the time evolution of the molecular charge Q_{mol} of Cl_2 exposed to the laser field of frequency $\omega=0.0746$ a.u., maximal amplitude $E_{\max}=0.6$ a.u., and pulse length [full width at half maximum (FWHM)] $\tau=20T$, where T denotes the optical period (2.03 fs). The former two correspond to wavelength $\lambda=610$ nm and a peak intensity of 1.3×10^{16} W/cm^2, respectively. Note that the amplitude of the electric field is maximum at $t=20T=40.7$ fs. The molecular charge Q_{mol} is defined as

$$Q_{\mathrm{mol}}=2Z-\int_{x_L-a}^{x_R+a}\rho(x)dx, \qquad a=3 \text{ a.u.} \tag{17}$$

The time evolution of the internuclear distance R is shown in Fig. 3.

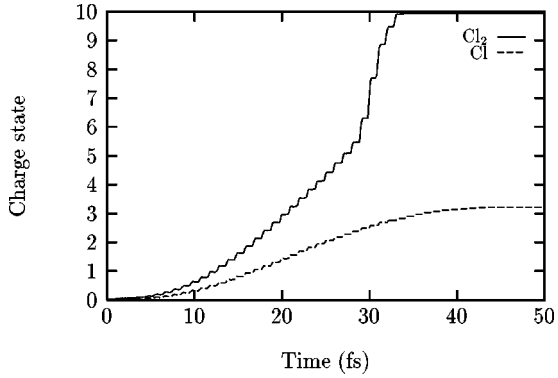

FIG. 2. Evolution of the molecular charge Q_{mol} of a Cl_2 molecule (solid line) and the degree of ionization of a Cl atom (dashed line) irradiated by the laser electric field with wavelength $\lambda=610$ nm, a peak intensity of 1.3×10^{16} W/cm^2 and a pulse length (FWHM) of $20T$, where T denotes the optical period (2.03 fs). Note that the laser intensity is maximum at $t=20T=40.7$ fs.

As soon as the laser is switched on at $t=0$, the molecule begins to be ionized. With the increase of laser field, the ionization proceeds gradually, while the internuclear distance hardly changes, since the molecule is trapped in a well of the potential-energy curve of a molecular ion. For example, the potential energy curve calculated using the one-dimensional Thomas-Fermi model for Cl_2^{2+} has a local minimum near the equilibrium internuclear distance of neutral molecules [12], which implies that Cl_2^{2+} is metastable. In fact, several theoretical [37,38] and experimental [38,39] studies have confirmed that Cl_2^{2+} and even Cl_2^{3+} are metastable. As the molecular charge reaches $Q_{\mathrm{mol}}\approx3.5$ at $t\approx22$ fs, the two nuclei begin to separate from each other due to Coulomb repulsion, while the ionization rate remains nearly constant in spite of the increasing laser electric field. At $t\approx29$ fs, where $R\approx4.15$ a.u., the ionization rate is suddenly enhanced. We can see that the ionization rate reaches its maximum at $t\approx30$ fs and that the enhanced ionization continues until $t\approx33$ fs, where $R\approx5.2$ a.u. Once the enhanced ionization has started, the internuclear distance R increases rapidly due to a strong Coulomb repulsion. After R has passed through the region of enhanced ionization, nearly no more ionization occurs. Thus ionization is completed before the laser intensity reaches its maximum at $t=40.7$ fs.

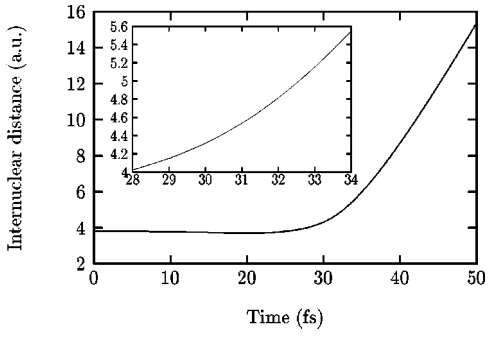

FIG. 3. Evolution of the internuclear distance R of a Cl_2 molecule irradiated by the same laser electric field as for Fig. 2. Inset: Expanded view of the region of enhanced ionization.

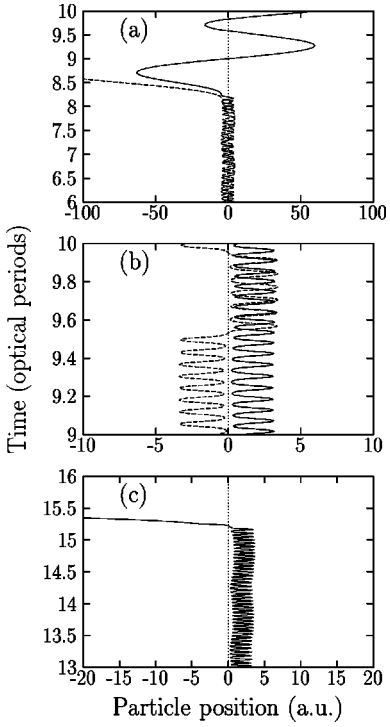

FIG. 4. Examples of test particle trajectories for the case of Fig. 2. (a) Two loosely bound particles. Initially they oscillate between two atomic wells, and are ejected from the outer wall of the left potential well. The particle with a solid line comes back to the molecule three times but passes through it and flies away. (b) A tightly bound (solid line) and an intermediately bound (dashed line) particles. (c) This test particle is initially localized in the right well and ejected beyond the internal potential barrier directly to the continuum.

We plot several typical test particle trajectories in Fig. 4. This figure illustrates the oscillation, ejection, and escape of test particles.

A. Ionization probability enhancement

Let us examine the enhancement of the ionization rate observed at $14T<t<17T$ (28 fs$<t<$34 fs) in more details. In order to check if this is caused simply by increasing laser electric field, we have simulated the ionization of a Cl atom in the same laser field (the dashed line of Fig. 2). In this case the ionization rate changes smoothly through the whole course of ionization. Moreover, the final charge state of the ions in the molecular case (5.0+ per ion) is significantly higher than in the atomic case (3.2+) in agreement with experimental findings [40]. These observations confirm that the sudden increase of ionization rate found in the molecular case is not due to the laser field increase. Several theoretical studies [6–11] have suggested that the ionization probability of diatomic molecules depends sensitively on the internuclear distance and peaks at some *critical distance* R_c larger than the equilibrium distance R_e. Constant and co-workers [41,42], in their experiments using pump-probe pulses with variable delays, confirmed that the ionization probability of a I_2^{2+} molecule depends strongly on its internuclear distance.

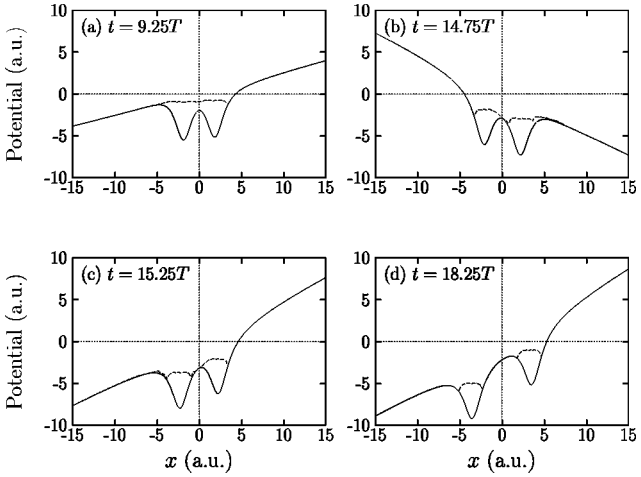

FIG. 5. Effective potential curves for the case of Fig. 2 at (a) $t=9.25T$, (b) $14.75T$, (c) $15.25T$, and (d) $18.25T$. Dashed lines represent the function $\Phi_{\rm eff}(x)+2A\rho(x)$, which is a measure of adiabaticity of the electron cloud (see text).

The appearance of the enhanced ionization can be related to the relative height of two barriers in the effective potential $\Phi_{\rm eff}$. Figure 5 shows the snapshots of the effective potential for the case of Fig. 2 at four different times. The two atomic potential wells are superposed on the linear potential of the oscillating electric field. In each snapshot we can see two potential barriers. Let us call the one between the two potential wells the internal barrier, and the other one the external barrier. In this figure, we have also plotted $\Phi_{\rm eff}(x)+2A\rho(x)$ with dashed lines. As can be seen from Eq. (13), this function has a constant value if $\Phi_{\rm eff}$ and ρ are the solutions of the Thomas-Fermi equations. Thus this function permits us to estimate how well the electron cloud adjusts itself to the instantaneous effective potential. This should not be, however, confused with the highest occupied energy level.

In the early stage of the ionization [see Fig. 5(a)], the internal potential barrier is lower than the external one. Loosely bound electrons are scarcely affected by the internal barrier and can move throughout the molecule [Fig. 4(a)], while the motion of tightly bound electrons is constrained in one potential well [Fig. 4(b) solid line]. In Fig. 4(c) we can also see that the originally intermediately bound test particle is affected by increasing laser field and becomes synchronized with it; it is localized in the left well during the first half-optical cycle and in the right well during the second half. In such a situation the electron cloud can adjust itself to the effective potential quite well, which is confirmed by the fact that the dashed line, representing $(\Phi_{\rm eff}+2A\rho)$, of Fig. 5(a) is nearly constant. This leads to charge oscillation in the molecule as is seen in Fig. 6. In this stage, stripping off of loosely bound charge (test particles) takes place mainly on the outer walls of the potential wells. Typical trajectories of ejected test particles are shown in Fig. 4(a).

At the beginning of the ionization rate enhancement [$14.75T$, Fig. 5(b)] the internal and external barriers are almost equally high, and later [$15.25T$, Fig. 5(c)] the internal barrier becomes higher than the external one. This leads to a qualitative change in ionization mechanism. The rising inter-

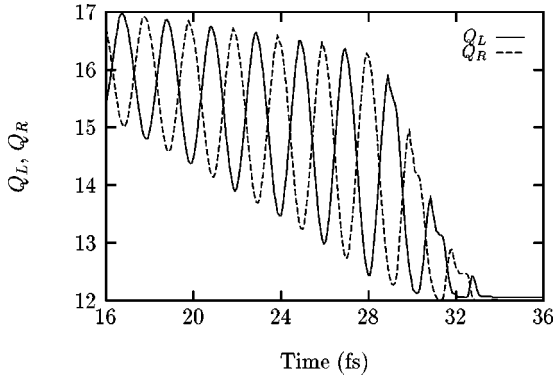

FIG. 6. Evolution of the electronic charges Q_L and Q_R belonging to the left and right nuclei, respectively, for the case of Fig. 2.

nal potential barrier disturbs the motion of test particles, and this results in a nonadiabatic localization of electronic charge in the upper well, which can be clearly seen from the dashed lines in Figs. 5(b) and 5(c). Here we use the term ''localization'' to mean that during the half-optical cycle a substantial part of electrons (or test particles) remain in the upper potential well rather than make an adiabatic transition to the lower well. Localization of a similar type was also reported in quantum-mechanical calculations of the ionization of the H_2^+ ion [8] and of diatomic molecules [6,7]. In this situation, adiabatic treatments of molecular ionization are no longer justified. Now if test particles localized in the upper atomic well are sufficiently energetic to overcome the internal barrier, they can directly escape the molecule to the continuum. This enhances the ionization probability dramatically. An example of trajectories of such escaping test particles is shown in Fig. 4(c). Let us note a qualitative difference between this trajectory and the ones in Fig. 4(a). In the former, the test particle is initially localized in one potential well and escapes the molecule across the other potential well.

The direct ''over-the-internal-barrier'' escape of the electrons can also be confirmed in Fig. 6, which shows the temporal behavior of the electronic charges belonging to the left (Q_L) and right (Q_R) nuclei. They are defined as

$$Q_L = \int_{x_L - a}^{x_m} \rho(x)dx, \quad Q_R = \int_{x_m}^{x_R + a} \rho(x)dx, \qquad (18)$$

where $x_m = (x_L + x_R)/2$. From this figure we can see that during the period of enhanced ionization, the decrease of the charge belonging to one nucleus does not entirely result in the increase of the charge belonging to the other nucleus. The missing charge has passed to the continuum. In Table I we list the times at which Q_L and Q_R reach local minima. Before the enhanced ionization begins, the minima are located near $t = (l + \frac{1}{4})T$ and $(l + \frac{3}{4})T$, where l is an integer. The electron cloud motion is in phase with the laser field. However, after $t = 14T$, the minima are seen to be delayed considerably with respect to the corresponding extrema of the laser field, which implies that the electron cloud cannot follow the laser field due to the rising internal potential barrier.

TABLE I. The times at which the electronic charges belonging to the left (Q_L) and right (Q_R) nuclei reach their local minima during the interval $9T < t < 16T$. They are given in T (optical periods).

Q_L	Q_R
8.78	8.27
9.77	9.27
10.76	10.27
11.77	11.27
12.77	12.26
13.78	13.27
14.85	14.32
15.90	15.37

By $t = 18.25T$ [Fig. 5(d)] all loosely and moderately bound electrons are gone, and the remaining charge is stuck in the atomic wells. In fact, we can see in Fig. 6 that the charge oscillation between the two wells has disappeared by this time. Thus ionization has been shut off.

In the above we have seen that the ionization probability is dramatically enhanced for the internuclear distance 4.15 a.u. $< R <$ 5.2 a.u. It should be noted, however, that only less than half of the ejected charge is stripped off during this interval, while more than four electrons are ejected before the nuclei separate from each other significantly. Moreover if we plot the molecular charge Q_{mol} as a function of the internuclear distance R (Fig. 7), we find that ionization event is not localized in quite a small range of R near R_c. It is true that the ionization probability is enhanced there, but the laser intensity is sufficiently high for ionization to proceed even before the internuclear distance reaches R_c, and the nuclei separate from each other rapidly due to strong Coulomb repulsion once the enhanced ionization begins. Hence the ionization occurs sequentially as the internuclear distance increases.

Let us make a brief remark on the kinetic energy of the resulting ion fragments. Although the final kinetic energy of the ions can be calculated in the present model, it is not of much use to compare it with experimental values, since we have assumed that the nucleus-electron and electron-electron

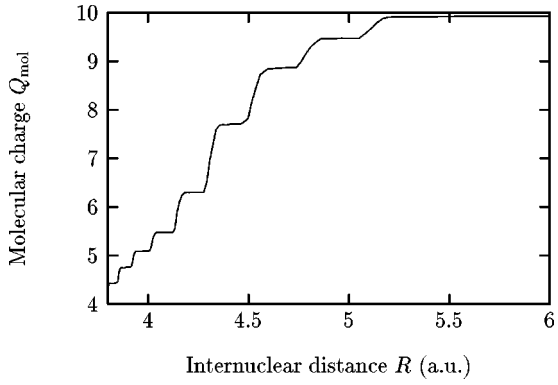

FIG. 7. Molecular charge Q_{mol} as a function of internuclear distance R (a.u.) for the case of Fig. 2.

interactions are expressed by a ''soft Coulomb'' potential as in Eq. (3), and not by a pure Coulomb potential. Thus we compare the critical distance R_c here. In most previous work, the critical distance R_c is obtained for each charge state from the evaluations of the ionization probability or of the threshold as a function of internuclear distance. Since the present model simulates the temporal evolution of ionization, we do not obtain the corresponding value of R_c. Nevertheless, from Figs. 2 and 3 we may say that the ionization rate reaches a maximum at $R \approx 4.4$ a.u., which may be taken as the value of R_c. Its ratio to R_e is 1.2. This is smaller than the values reported in the previous work [6–11], and it alone cannot completely explain the kinetic-energy defect observed experimentally. Moreover, since a Cl_2 molecule is triply ionized almost at R_e, the kinetic-energy defect for $Cl_2{}^{3+} \rightarrow Cl^+ + Cl^{2+}$ and $Cl_2{}^{4+} \rightarrow Cl^{2+} + Cl^{2+}$ channels [4] cannot be understood in terms of enhanced ionization. The kinetic-energy defect probably stems not only from ionization taking place preferably at a critical distance larger than R_e, but also from the fact that real potential-energy curves of molecular ions are different from Coulombic ones $(q_1 q_2 / R)$. Safvan and Mathur [43] showed that dissociation via non-Coulombic potential-energy curves of $N_2{}^{q+}$ yields lower values of kinetic energies than would be expected from calculations using purely Coulombic potentials. Theoretical calculations of potential energy curves of $Cl_2{}^{q+}$ [37] and $I_2{}^{q+}$ [42] using multireference configuration interaction methods have revealed that there are significant energy defects from the corresponding Coulombic curves, due to residual chemical bonding.

B. Comparison with the hydrodynamic model

Our model of the MEDI of diatomic molecules allows us to deal with all the electrons and nuclei explicitly. To the authors' knowledge, the only such approach which was previously published is the hydrodynamic model based on the time-dependent Thomas-Fermi theory [12–14]. Interestingly our results are qualitatively different from those in Refs. [12–14].

One remarkable result of the hydrodynamic simulations is that the ejected electron cloud does not expand rapidly and that the screening of the ion fragments by this electron cloud may be sufficient to explain the kinetic-energy defect. On the contrary, in our results, ejected test particles rapidly move away from the molecule, as can be seen in Figs. 4(a) and 4(c). It is true that some of ejected test particles return to the molecule in the oscillating electric field, but they are in most cases so energetic that they just pass through the molecule and go away [see Fig. 4(a), solid line]. As a simple model, let us consider the motion of a free electron in an oscillating electric field $E_0 \sin \omega t$. If its position and velocity at $t=0$ are x_0 and v_0, respectively, its position x as a function of t is given by

$$x(t) = x_0 + \frac{E_0}{\omega^2} \sin \omega t + \left(v_0 - \frac{E_0}{\omega} \right) t. \tag{19}$$

The second and third terms on the right-hand side represent the oscillation and drift, respectively. We have found that the motion of ejected test particles can be roughly modeled by this equation. For $E_0 = 0.3$ a.u. $(= E_{\max}/2)$ and $\omega = 0.0746$ a.u., the oscillation amplitude is $E_0/\omega^2 = 54$ a.u., and the second term of the drift velocity is $E_0/\omega = 4.0$ a.u., which corresponds to a drift of 34 a.u. per optical period. Hence ejected test particles readily move away from the molecule. As a consequence, the screening of the ion fragments by an enclosed electron cloud is not observed in our model.

In the hydrodynamic model, it is assumed that interactions between electrons are so dominant that the electron gas is in local thermodynamic equilibrium at each moment [44]. This assumption may be questionable for a description of the ejected charge. Under such an assumption, even if an electron is accelerated by a laser field, it is immediately decelerated through interactions with neighboring electrons. This may explain why the electron cloud does not expand rapidly, and why the enhancement of ionization probability is not observed in the hydrodynamic model. On the other hand, our PIC model describes the situation where electrons undergo few collisions. Such test particles that have obtained sufficient energy from the laser field can readily escape from the molecule. Moreover, our model, based on the Vlasov equation, allows test particles of different velocities to reside near one another, in contrast with the hydrodynamic approach. We believe that these facts make our approach more suitable for modeling the ionization of molecules in an intense laser field.

It should be stressed that the above discussion is not to deny possible roles of the screening by *bound* electrons. In fact, we consider that the experimentally observed kinetic-energy defect is caused by a combination of ionization taking place preferably at a critical distance larger than the equilibrium internuclear distance and of significant charge-density distributions of bound electrons (not of ejected free electrons) in the internuclear region, as we mentioned at the end of Sec. III A

IV. ENHANCED IONIZATION IN A TRIATOMIC MOLECULE

In Sec. III we have seen that the laser interaction with diatomic molecules (Cl_2) yields ions of much higher charge than in case of atoms (Cl) thanks to enhanced ionization. Now the question arises of whether ionization is further enhanced in the case of triatomic linear molecules. If the ionization mechanism in a triatomic molecule is similar to the diatomic case, the yields of highly charged ions will be similar for diatomic and triatomic molecules. Conversely, if a qualitatively different mechanism appears due to the interplay of the three atomic wells, it is expected that higher charge state is observed in triatomic molecules than in diatomics.

We have performed PIC simulations for a linear triatomic molecule in an intense laser field. It is straightforward to extend the simulation method described in Sec. II to a triatomic molecule. As a model molecule we have chosen a fictitious Cl_3 molecule composed of three Cl nuclei situated on a line in equilibrium with the same distance as the equi-

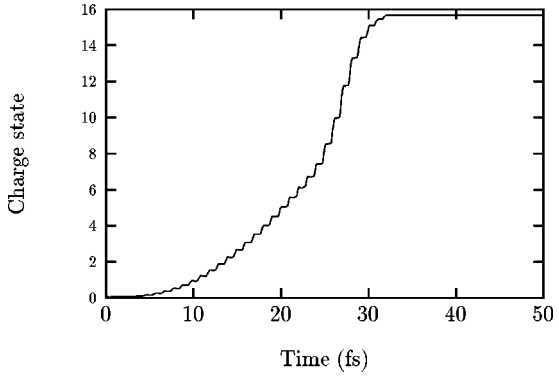

FIG. 8. Evolution of the molecular charge Q_{mol} of a Cl_3 irradiated by the same laser electric field as for Fig. 2.

librium internuclear distance (3.8 a.u.) of Cl_2. We also use the same values of the parameters A, b, and c as before. Although these choices might appear to be unrealistic, they enable us to compare directly the ionization behavior of a diatomic and a triatomic molecule, excluding effects stemming from other factors such as different bond lengths and constituting atoms. The results shown in this section have been obtained with the test particle number $N_p = 750\,000$.

Figure 8 shows the time evolution of the molecular charge Q_{mol} of Cl_3 exposed to the same laser field as for Fig. 2. Similarly to Eq. (17) it is defined as

$$Q_{\mathrm{mol}} = 3Z - \int_{x_L - a}^{x_R + a} \rho(x)\,dx, \qquad a = 3 \text{ a.u.}, \tag{20}$$

where $Z = 17$. We can see the signal of enhanced ionization for $12T < t < 16T$ (24 fs $< t <$ 32 fs), and the final value of Q_{mol} is 15.7. In Table II we summarize the final ion charge states for the cases of Cl, Cl_2, and Cl_3. This table tells us that the ion charge obtained in the laser irradiation of linear triatomic molecules are only slightly higher than in case of diatomic molecules while in the latter much more highly charged ions are yielded than in case of atoms. This observation is in agreement with the finding in recent experiments [20].

In order to examine the mechanism of enhanced ionization in triatomic molecules, in Fig. 9 we plot the effective potential Φ_{eff} (solid lines) and the function $\Phi_{\mathrm{eff}}(x) + 2A\rho(x)$ (dashed lines) at three different times. The latter is a measure of adiabaticity of the electron cloud as we discussed in Sec. III A. This time each snapshot has three potential barriers: two internal and one external.

In the early stage of the ionization [$9.25T$, Fig. 9(a)], the internal barriers are lower than the external one. The dashed

TABLE II. The charge states of ion fragments from Cl, Cl_2, and Cl_3.

Atom or molecule	Charge state
Cl	3.2
Cl_2	4.9 (left), 5.0 (right)
Cl_3	5.6 (left), 4.6 (center), 5.5 (right)

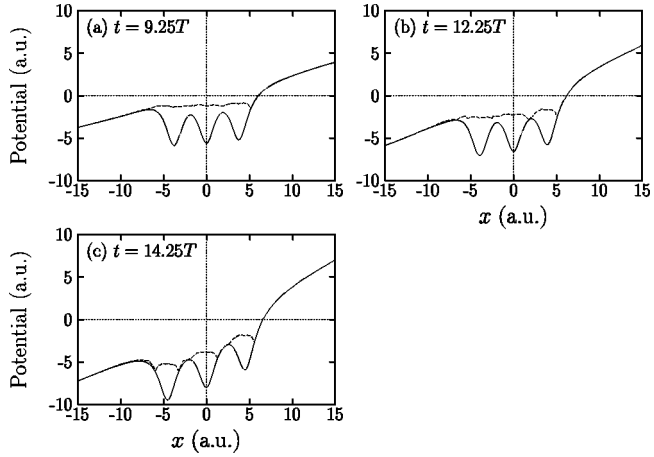

FIG. 9. Effective potential curves for the case of Fig. 8 at (a) $t = 9.25T$, (b) $12.25T$, and (c) $14.25T$. Dashed lines represent the function $\Phi_{\mathrm{eff}}(x) + 2A\rho(x)$, which is a measure of the adiabaticity of the electron cloud.

line is nearly constant: the electron cloud can adjust itself to the effective potential relatively well. At the beginning of enhanced ionization [$12.25T$, Fig. 9(b)], the right internal barrier becomes higher than the external one, while the left internal one is still lower than the external one. In such a situation, the motion of loosely bound electrons are perturbed by the right internal barrier, and electronic localization occurs in the highest potential well [the rightmost well in Fig. 9(b)]. The left internal potential barrier is not sufficiently high to perturb significantly the electronic motion between the left two potential wells. These can be seen from the fact that the dashed line is relatively constant through the left two wells, while it is higher in the rightmost well. Thus the lowest and central atomic wells behave like one potential well as a whole. If test particles localized in the highest atomic well have sufficient energy to overcome the right internal potential barrier, they can directly escape the molecule to the continuum, which leads to the enhancement of ionization. At $t = 14.25T$ [Fig. 9(c)] the lower internal barrier surpasses the external barrier, and hinders the motion of loosely bound test particles between the lowest two atomic wells. The resulting nonadiabatic electronic charge localization in the central well as well as in the highest well again leads to ionization enhancement.

It was argued in Ref. [21] that in a stage corresponding to Fig. 9(b) the one-step ''through-the-internal-barrier'' ionization from the middle potential well is not possible, and that ionization takes place via the resonance tunneling mechanism. It is also argued that in a later stage corresponding to Fig. 9(c) the through-the-internal-barrier mechanism following the localization of the charge in the middle potential well is a main channel of ionization. In both stages, Seideman *et al.* [21] did not refer to the possibility of ionization from the highest potential well. Our results, on the other hand, show that the ''over-the-internal-barrier'' ionization from the highest potential well is possible in both stages. In particular, this is a main ionization mechanism in the early stage of enhanced ionization [Fig. 9(b)], where the lower internal barrier is still lower than the external barrier. Due to this fact,

the ionization enhancement is triggered at a smaller internuclear distance (3.95 a.u.) than in the diatomic case (4.15 a.u.). Although our model, in which the motion of test particles is classical, does not include tunnel effect, its results imply that the through-the-internal-barrier ionization from the highest potential well may exist in quantum-mechanical situations.

It should be noted that, although all three atomic wells do participate in ionization enhancement, as we have seen above, its mechanism is essentially the same as in a diatomic molecule: nonadiabatic (partial) localization of electronic charge in higher potential wells due to rising internal potential barriers and the direct over-the-internal-barrier escape of the localized charge to the continuum. This explains that there is little further ionization enhancement in a linear triatomic molecule with respect to the diatomic case.

V. CONCLUSIONS

We have presented a one-dimensional particle-in-cell (PIC) simulation of multielectron dissociative ionization (MEDI) of a Cl_2 molecuse and a fictitious Cl_3 molecule in an intense laser field. In our model the dynamics of all the electrons and nuclei is taken into account. The effects of quantum mechanics are partially included in the initial electron density distribution, which is calculated from a one-dimensional Thomas-Fermi model. The present model enables us to follow the evolution of the MEDI process dynamically.

In simulations for a Cl_2 molecule, we have reconfirmed that the ionization rate is strongly enhanced at a certain range of internuclear distance. To the authors' knowledge, the present dynamical model is the first to confirm the existence of enhanced ionization by treating all the electrons and nuclei explicitly. The enhanced ionization is connected to the rise of the internal barrier of the effective potential and the resulting nonadiabatic localization of electrons in the upper potential well. However, the internuclear distances at which ionization events take place are not necessarily localized at the critical distance but are distributed over a relatively wide range. In view of the relative smallness of the critical distance obtained in our simulations, we consider that experimentally observed kinetic-energy defects are caused by a combination of the enhanced ionization at a critical distance larger than the equilibrium internuclear distance and the non-Coulombic nature of the potential energy curves of Cl_2^{q+}. Our results do not support the idea of the ejected-electron screening of ion fragments. In our model the ejected electrons rapidly fly away from the molecule. Such a dynamic screening, proposed in Refs. [12–14], may be an artifact due to the application of the hydrodynamic approach to the MEDI process.

In the comparison of ionization behavior of Cl_2 and Cl_3, we have found that the final charge state of the ion fragments from the triatomic molecule is not increased significantly with respect to the diatomic case, in agreement with experimental findings [20]. All three potential wells are involved in ionization enhancement in a linear triatomic molecule. In particular, ionization from the highest potential well, which was not mentioned in the previous work [21], has been found to occur. The mechanism of the enhanced ionization in a linear triatomic molecule is similar to the case of a diatomic molecule. Although we have applied our model to diatomic and triatomic molecules, it is straightforward to extend the model to treat multiatomic molecules or to small clusters.

ACKNOWLEDGMENTS

The preliminary version of the code used in the present study was programmed by M. Brewczyk. We would also like to thank him for many fruitful discussions. We wish to express our gratitude to M. Schmidt for a critical reading of the manuscript and for valuable comments. Thanks are due to Ph. Hering and C. Cornaggia for enlightening us on the experimental aspects. We are indebted to L. Plagne for providing us with a copy of his thesis [33].

APPENDIX: SCALING PROPERTY

One of the elegant features of the original Thomas-Fermi model [45,46] of an atom is that the electron density and the atomic potential scale with atomic number Z. Photoabsorption spectra of an atom [47] and an ion in a plasma [48] calculated within the framework of linearized Bloch's hydrodynamic equations combined with the Thomas-Fermi theory also has a scaling property with Z. As for the one-dimensional version of the model, it scales not only with Z but also with respect to the smoothing parameters b and c [13]. In this appendix we show that the dynamical model used in the present study also scale with respect to the atomic number and the smoothing parameters.

Let us first change the atomic number from Z to $\overline{Z}=\alpha Z$, where α is an arbitrary positive constant. It can be easily shown that if $\Phi(x)$ and $\rho(x)$ are the solutions of Eqs. (13) and (14) with $\Phi_0=0$, then the scaled potential $\overline{\Phi}(x)=\alpha\Phi(x)$ and density $\overline{\rho}(x)=\alpha\rho(x)$ are the solutions of the same equations corresponding to atomic number $\overline{Z}$. Consistently, the density $\overline{\rho}_j$ on grid j calculated from Eq. (1) with $\overline{Z}$ in place of Z satisfies $\overline{\rho}_j=\alpha\rho_j$. If we multiply Eqs. (2) and (3) by α and define, $\overline{t}=t/\sqrt{\alpha}$, $\overline{\Phi}_{\rm eff}=\alpha\Phi_{\rm eff}$, $\overline{E}(\overline{t})=\alpha E(t)$, $\overline{f}_i=\alpha f_i$, and $\overline{v}_i=\sqrt{\alpha}v_i$, we obtain

$$\frac{dx_i}{d\overline{t}}=\overline{v}_i, \qquad \frac{d\overline{v}_i}{d\overline{t}}=\overline{f}_i=-\frac{\partial}{\partial x}\overline{\Phi}_{\rm eff}(x_i,\overline{t}), \tag{A1}$$

$$\overline{\Phi}_{\rm eff}(x,\overline{t})=-\frac{\overline{Z}}{\sqrt{b^2+(x-x_L)^2}}-\frac{\overline{Z}}{\sqrt{b^2+(x-x_R)^2}}+\int_{-\infty}^{\infty}\frac{\overline{\rho}(x')}{\sqrt{c^2+(x-x')^2}}dx'+x\overline{E}(t). \tag{A2}$$

These equations have the same forms as Eqs. (2) and (3). This implies that if the $x_i(t)$'s are the test particle trajectories

for the atomic number Z and the electric field $E(t)$, the $x_i(\sqrt{\alpha}t)$'s are the trajectories for the atomic number αZ and the electric field $\alpha E(\sqrt{\alpha}\,t)$.

Let us next examine the scaling property with respect to the smoothing parameters b and c. We change b and c by the common factors $b \to \tilde{b} = \beta b$ and $c \to \tilde{c} = \beta c$, where β is again an arbitrary positive constant. Accordingly, we scale $\tilde{x} = \beta x$ and $\tilde{R} = \beta R$. If we set $\tilde{\Phi}(\tilde{x}) = \Phi(x)/\beta$, $\tilde{\Phi}_0 = \Phi_0/\beta$, and $\tilde{\rho}(\tilde{x}) = \rho(x)/\beta$, Eqs. (13) and (14) lead to

$$\tilde{\Phi}(\tilde{x}) + 2A\tilde{\rho}(\tilde{x}) = \tilde{\Phi}_0, \tag{A3}$$

$$\tilde{\Phi}(\tilde{x}) = -\frac{Z}{\sqrt{\tilde{b}^2 + (\tilde{x} - \tilde{R}/2)^2}} - \frac{Z}{\sqrt{\tilde{b}^2 + (\tilde{x} + \tilde{R}/2)^2}} - \int_{-\infty}^{\infty} \frac{\tilde{\rho}(\tilde{x}')}{\sqrt{\tilde{c}^2 + (\tilde{x} - \tilde{x}')^2}} d\tilde{x}'. \tag{A4}$$

Thus, if we know the Thomas-Fermi potential $\Phi(x)$ for the smoothing parameters a and b and the initial internuclear distance R, we readily obtain the corresponding potential for the parameters βb, βc, and βR by $(1/\beta)\Phi(x/\beta)$. The introduction of the scaled quantities $\tilde{t} = \beta^{3/2} t$, $\tilde{\Phi}_{\rm eff}(\tilde{x}, \tilde{t}) = \Phi_{\rm eff}(x,t)/\beta$, $\tilde{f}_i = f_i/\beta^2$, $\tilde{v}_i = v_i/\sqrt{\beta}$, and $\tilde{E}(\tilde{t}) = E(t)/\beta^2$ allows us to rewrite Eqs. (2) and (3) as

$$\frac{d\tilde{x}_i}{d\tilde{t}} = \tilde{v}_i, \qquad \frac{d\tilde{v}_i}{d\tilde{t}} = \tilde{f}_i = -\frac{\partial}{\partial \tilde{x}} \tilde{\Phi}_{\rm eff}(\tilde{x}_i, \tilde{t}). \tag{A5}$$

$$\tilde{\Phi}_{\rm eff}(\tilde{x}, \tilde{t}) = -\frac{Z}{\sqrt{\tilde{b}^2 + (\tilde{x} - \tilde{x}_L)^2}} - \frac{Z}{\sqrt{\tilde{b}^2 + (\tilde{x} - \tilde{x}_R)^2}} + \int_{-\infty}^{\infty} \frac{\rho(\tilde{x}')}{\sqrt{\tilde{c}^2 + (\tilde{x} - \tilde{x}')^2}} d\tilde{x}' + \tilde{x}\tilde{E}(\tilde{t}), \tag{A6}$$

These equations have again the same forms as Eqs. (2) and (3). Therefore, we can express the particle trajectories in the laser field $E(t/\beta^{3/2})/\beta^2$ for smoothing parameters $\tilde{b}$ and $\tilde{c}$ and the initial internuclear distance $\tilde{R}$ as $\beta x_i(t/\beta^{3/2})$, once the trajectories $x_i(x)$ in the field $E(t)$ are obtained for the corresponding parameters b, c, and R.

[1] L.J. Frasinski, K. Codling, P. Hatherly, J. Barr, I.N. Ross, and W.T. Toner, Phys. Rev. Lett. **58**, 2424 (1987).

[2] K. Boyer, T.S. Luk, J.C. Solem, and C.K. Rhodes, Phys. Rev. A **39**, 1186 (1989).

[3] D.T. Strickland, Y. Beaudoin, P. Dietrich, and P.B. Corkum, Phys. Lett. **68**, 2755 (1992).

[4] M. Schmidt, D. Normand, and C. Cornaggia, Phys. Rev. A **50**, 5037 (1994).

[5] M. Schmidt, P. D'Oliveira, P. Meynadier, D. Normand, and C. Cornaggia, J. Nonlinear Opt. Phys. Mater. **4**, 817 (1995).

[6] T. Seideman, M.Y. Ivanov, and P.B. Corkum, Phys. Rev. Lett. **75**, 2819 (1995).

[7] M. Ivanov, T. Seideman, P. Corkum, F. Ilkov, and P. Dietrich, Phys. Rev. A **54**, 1541 (1996).

[8] T. Zuo and A.D. Bandrauk, Phys. Rev. A **52**, R2511 (1995).

[9] D.M. Villeneuve, M.Y. Ivanov, and P.B. Corkum, Phys. Rev. A **54**, 736 (1996).

[10] J.H. Posthumus, A.J. Giles, M.R. Thompson, W. Shaikh, A.J. Langley, L.J. Frasinski, and K. Codling, J. Phys. B **29**, L525 (1996).

[11] J.H. Posthumus, A.J. Giles, M.R. Thompson, and K. Codling, J. Phys. B **29**, 5811 (1996).

[12] M. Brewczyk, K. Rzążewski, and C.W. Clark, Phys. Rev. Lett. **78**, 191 (1997).

[13] M. Brewczyk and K. Rzążewski, Phys. Rev. A **60**, 2285 (1999).

[14] M. Brewczyk and K. Rzążewski, Phys. Rev. A **61**, 023412 (2000).

[15] J. Grochmalicki, M. Lewenstein, and K. Rzążewski, Phys. Rev. Lett. **66**, 1038 (1991).

[16] M. Gajda, J. Grochmalicki, M. Lewenstein, and K. Rzążewski, Phys. Rev. A **46**, 1638 (1992).

[17] K. Rzążewski, M. Lewenstein, and P. Salières, Phys. Rev. A **49**, 1196 (1994).

[18] P.B. Corkum, Phys. Rev. Lett. **71**, 1994 (1993).

[19] S. Augst, D. Strickland, D.D. Meyerhofer, S.L. Chin, and J.H. Eberly, Phys. Rev. Lett. **63**, 2212 (1989).

[20] Ph. Hering and C. Cornaggia, Phys. Rev. A **57**, 4572 (1998).

[21] T. Seideman, M.Yu. Ivanov, and P.B. Corkum, Chem. Phys. Lett. **252**, 181 (1996).

[22] D. Normand, L.A. Lompré, and C. Cornaggia, J. Phys. B **25**, L497 (1992).

[23] P.A. Hatherly, L.J. Hatherly, K. Codling, A.J. Langley, and W. Shaikh, J. Phys. B **23**, L291 (1990).

[24] P.D. Dietrich, D.T. Strickland, M. Laberge, and P.B. Corkum, Phys. Rev. A **47**, 2305 (1993).

[25] J. Javanainen, J.H. Eberly, and Q. Su, Phys. Rev. A **38**, 3430 (1988).

[26] Q. Su, J.H. Eberly, and J. Javanainen, Phys. Rev. Lett. **64**, 862 (1990).

[27] J. H. Eberly, R. Grobe, C. K. Law, and Q. Su, in *Atoms in Intense Laser Fields*, edited by M. Gavrila (Academic Press, Orlando, FL, 1992), p. 301.

[28] K.C. Kulander, F.H. Mies, and K.J. Schafer, Phys. Rev. A **53**, 2562 (1996).

[29] C. K. Birdsall and A. B. Langdon, *Plasma Physics via Computer Simulation* (McGraw-Hill, New York, 1985).

[30] M. P. Allen and D. J. Tildesley, *Computer Simulation of Liquids* (Clarendon, Oxford, 1987).

[31] A. Pukhov and J. Meyer-ter-Vehn, Phys. Rev. Lett. **79**, 2686 (1997).

[32] R.L. Morse, and C.W. Nielson, Phys. Fluids **12**, 2418 (1969).

[33] L. Plagne, Ph.D. thesis, Université de Grenoble, Grenoble, France (1999).

[34] M. Brack and R. K. Bhaduri, *Semiclassical Physics* (Addison-Wesley, Reading, MA, 1997), p. 151.
[35] P. Ring and P. Schuck, *The Nuclear Many Body Problem* (Springer, New York, 1980).
[36] G. Herzberg, *Molecular Spectra and Molecular Structure*, Spectra of Diatomic Molecules Vol. I (Van Nostrand, Princeton, 1950).
[37] J.S. Wright, G.A. DiLabio, D.R. Matusek, P.B. Corkum, M.Yu. Ivanov, Ch. Ellert, R.J. Buenker, A.B. Alekseyev, and G. Hirsch, Phys. Rev. A **59**, 4512 (1999).
[38] H. Sakai, H. Stapelfeldt, E. Constant, M.Yu. Ivanov, D.R. Matusek, J.S. Wright, and P.B. Corkum, Phys. Rev. Lett. **81**, 2217 (1998).
[39] J.H. Beynon, R.M. Caprioli, and J.W. Richardson, J. Am. Chem. Soc. **21**, 1852 (1971).
[40] D. Normand and M. Schmidt, Phys. Rev. A **53**, R1958 (1996).
[41] E. Constant, H. Stapelfeldt, and P.B. Corkum, Phys. Rev. Lett. **76**, 4140 (1996).
[42] Ch. Ellert, H. Stapelfeldt, E. Constant, H. Sakai, J. Wright, D.B. Rayner, and P.B. Corkum, Philos. Trans. R. Soc. London, Ser. A **356**, 329 (1998).
[43] C.P. Safvan and D. Mathur, J. Phys. B **27**, 4073 (1994).
[44] D. Potter, *Computational Physics* (Wiley, London, 1973), p. 155.
[45] L. D. Landau and E. M. Lifshitz, *Quantum Mechanics* (Pergamon, London, 1965), pp. 241–246.
[46] B. G. Englert, *Semiclassical Theory of Atoms*, Lecture Notes in Physics Vol. 300 (Springer, Berlin, 1988).
[47] J.A. Ball, J.A. Wheeler, and E.L. Firemen, Rev. Mod. Phys. **45**, 333 (1973).
[48] K. Ishikawa, B.U. Felderhof, T. Blenski, and B. Cichocki, J. Plasma Phys. **60**, 787 (1998).